Contact of rotors of screw machines

Ass. Prof. **Jaromír Švígler**, University of West Bohemia, Pilsen

Abstract
The main purpose of this contribution is to bring a new view on the contact properties of the liquid injected screw machines in an operating state in comparison with contact in the ideal state. The presented analysis is performed on the presumption of unchangeable shape of the rotors and deformable machine housing in course of the operating state. In an ideal state the axis rotors are parallel and the rotors touch each other in a curve in regard to their expected rigidity. In this case it is possible to solve kinematical and some static and dynamical problems as planar problems in the cross sections perpendicular to the rotor axes. In an operating state the parallel arrangement of the rotors axis changes into a general position and tooth surface of rotors touch each other at a point. This change of an arrangement of the axes of rotors causes a deviation ratio which necessarily leads to kinematics excitation of the rotors. Another consequence of this phenomenon is increased contact pressure in the small surface of the touch point. The mentioned problems have to be solved as a spatial problem.

1. Introduction

For the analysis of contact of the rotors it was necessary to create the mathematical models of the rotors and the housing of the screw machines. In an ideal state the axes of rotors, **Fig. 1**,

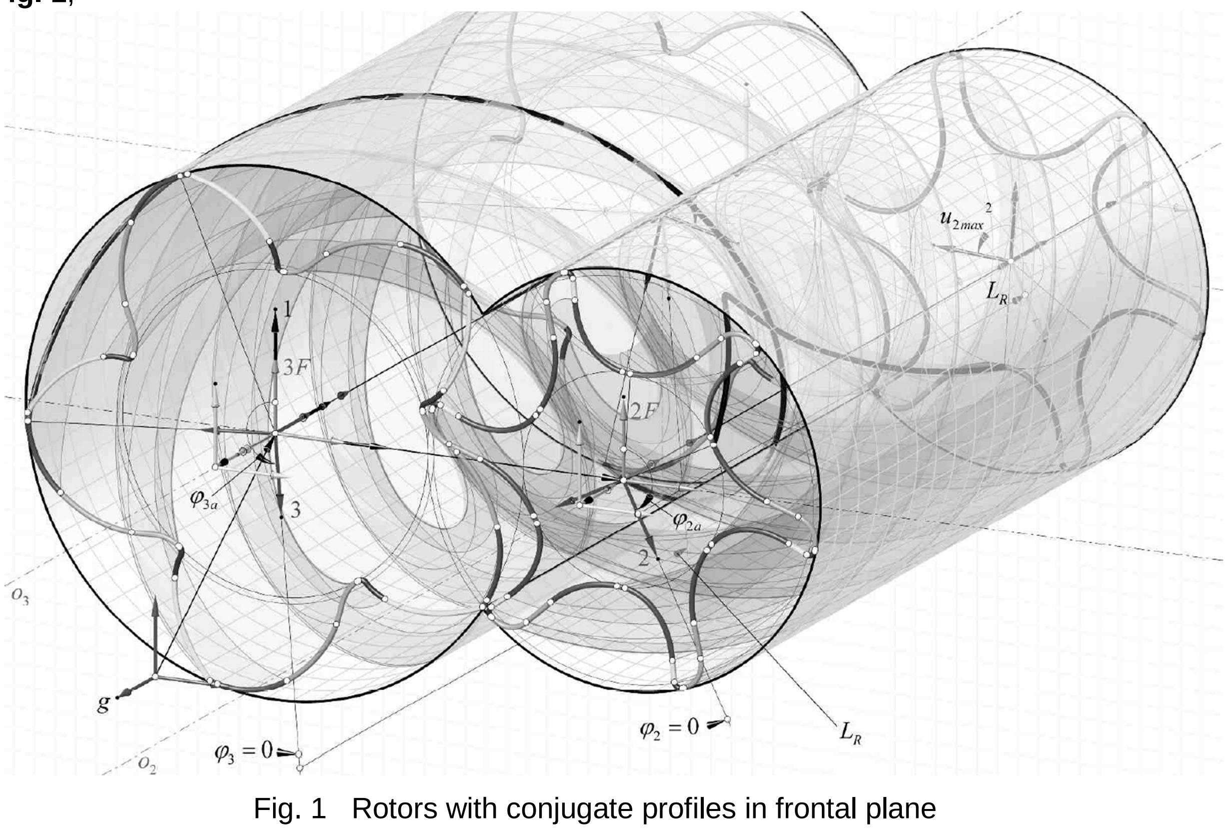

Fig. 1 Rotors with conjugate profiles in frontal plane

are parallel and their tooth surfaces create the higher kinematic pair. Both surfaces touch each other in a closed curve. Tooth surfaces, **Fig. 1**, have complicated shape and consist of envelopes and trochoidal curves. The working space of the screw machines is bounded by the tooth surfaces. The contact force between the rotors has an important role in the screw machines with direct contact between teeth. In the theoretical position of rotors, when their axes are parallel, the forces and therefore also the stress in the points of the contact curve are relatively small. The Situation is different in the case of breach of an ideal rotor seating when the contact between rotors takes place in the instantaneous isolated points. In this case the contact force is substantially larger [4]. The housing geometrical model, **Fig. 2**, was obtained in accordance with the real machine housing, **Fig. 3**, in the CAD system. The model is described parametrically as a whole i.e. each model detail is fully analytically described. Bearing elastic displacements are calculated in accordance with [6] and results were checked with the FEM software ANSYS [4]. On the input side, i.e. front side, **Fig. 2**, there are the radial roller bearings with cylindrical roller elements with zero of contact angle. On the output side there are the radi-axial roller bearings with tapered roller elements with non zero-contact angle.

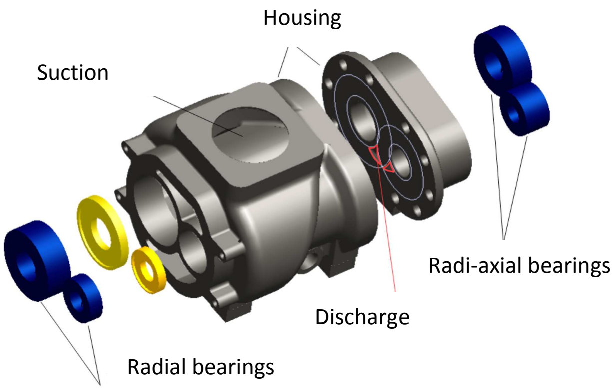

Fig. 2 Model of casing of screw machines compressor

Fig. 3 Real housing of screw compressor

2. Operating deformation housing and rotors

Deformation of the casing and screw machine rotors are caused by the force and thermal stress.

Force field

Force field of a screw compressor is primarily given by pressure of compressed medium in chambers [2]. Pressures in separated chambers of the working space were replaced by elementary forces at twelve time levels, in which the working cycle was divided, **Fig. 4**. Time level is given by the angle of rotation of the main rotor. These force fields were replaced by force screws, wrenches, $\rho_k\left(F_k, M_{ok}\right)$, **Fig. 5**, which represent forces and torques. The wrenches affecting in points, $E_k, k = 2, 3$, which are determined by the position vectors [1]

$$\mathbf{r}_{E_k} = \frac{\mathbf{F}_k \times \mathbf{M}_k}{|\mathbf{F}_k|} , \qquad (1)$$

where $\mathbf{F}_k = \sum_{i=1}^{n} \mathbf{F}_{k_i}$, $\mathbf{M}_k = \sum_{i=1}^{n} \mathbf{M}_{k_i}$ are the resulting effects on an elementary area of tooth surfaces. In Figure 5 the situation at maximum pressure just before the opening of the discharge channel, $\varphi_3 = 72^\circ$, is plotted.

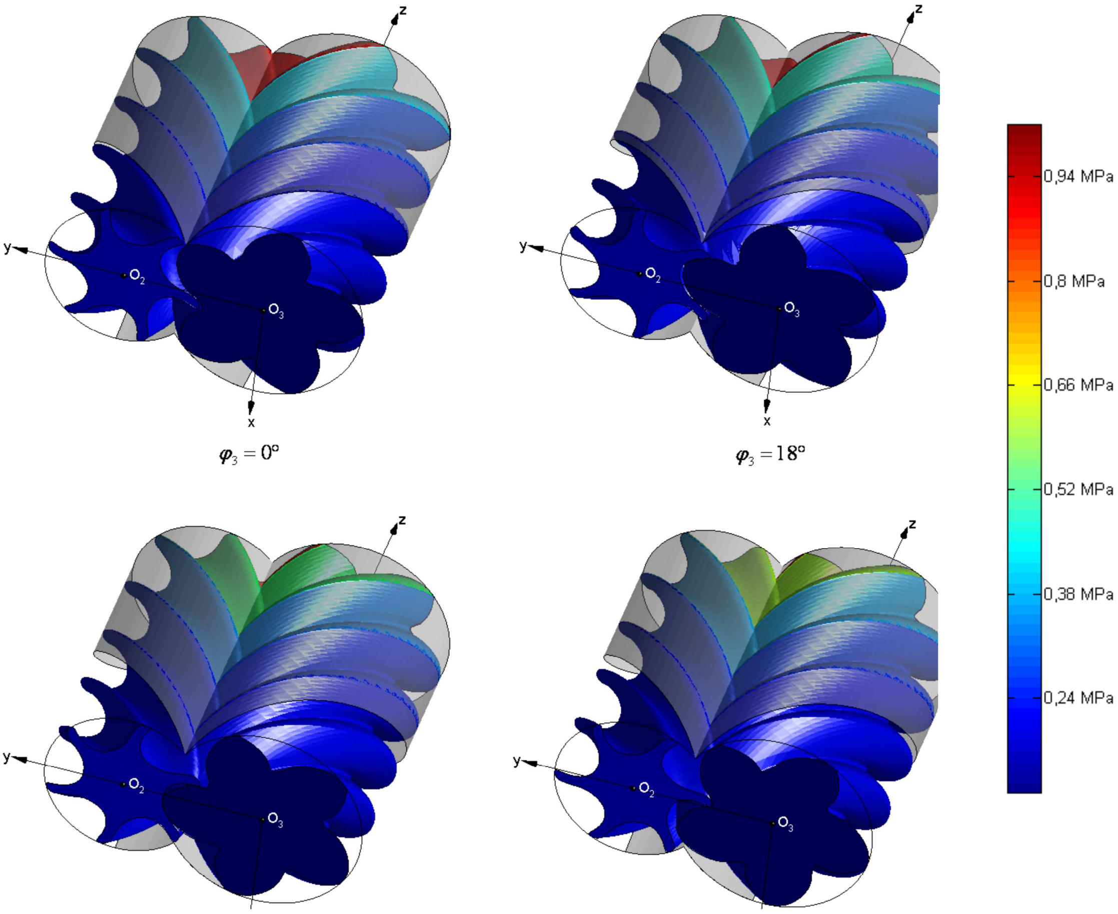

Fig. 4   Pressures in chambers for four time levels, view from bottom

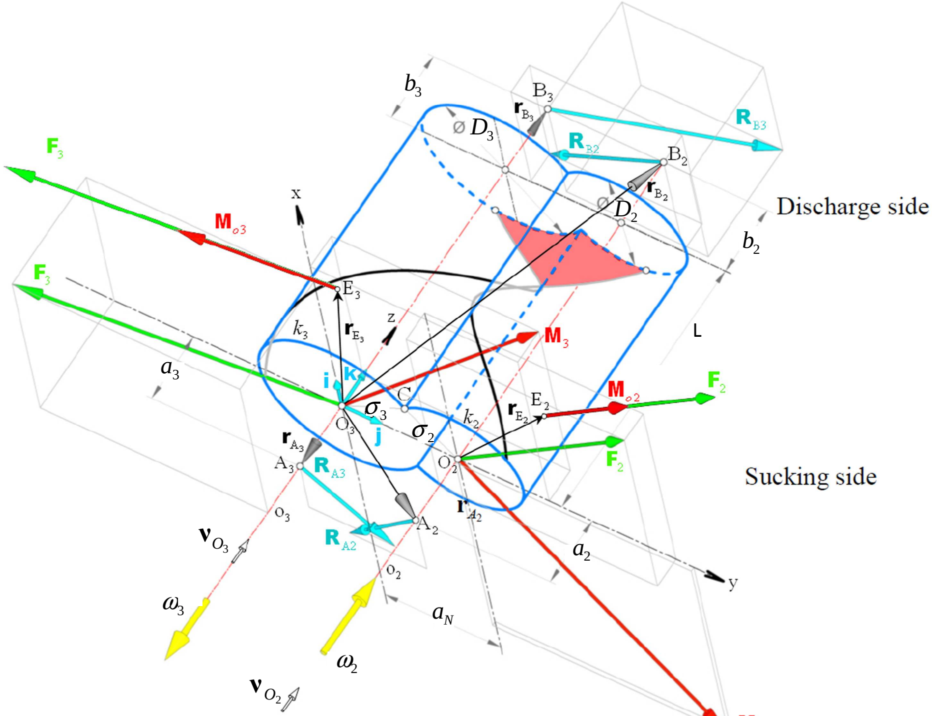

Fig. 5   Wrenches and reaction forces at bearings of rotors

In consequence of the deformation of the screw machine casing the rotor axes are moved into a skew position, and the initial curve contact is changed to the point of contact. In addition to the effect of the pressure force field, also the reaction force in the place of rotor bearing and the normal force between the rotor teeth acting on the rotors take effect. Size reaction forces depend on the position of the point of contact of tooth surfaces, which depends on the deformation of the casing which is retroactively influenced by reaction forces. This is a coupled problem which we have to solve as an iterative process:

- for $\varphi_3 = 0^\circ$, according to static equilibrium equations (2), we determine reaction forces, Fig. 5, in the bearings of the rotors using the fictitious moment

$$\mathbf{F}_j + \mathbf{R}_{A_j} + \mathbf{R}_{B_j} = \mathbf{0} \ ,$$

$$\left(\mathbf{r}_{B_j} - \mathbf{r}_{A_j}\right) \times \mathbf{R}_{B_j} + \mathbf{r}_{A_j} \times \mathbf{F}_j + \mathbf{M}_{A_j} + \mathbf{M}_{S_j} = \mathbf{0}, \quad j = 2, 3 \ , \tag{2}$$

  where $\mathbf{M}_{S_i}$ is an imaginary moment of a force couple added to the equation for equilibrium,

- deformation of casing is determined,
- the position vector ${}^{(0)}\mathbf{r}_E$ of the point of contact is determined,
- using the known position ${}^{(0)}\mathbf{r}_E$ of the touch point the reaction forces in the bearings are determined,
- the displacements of the bearing centres are determined,
- the position vector ${}^{(1)}\mathbf{r}_E$ of the point of contact is determined,
- if the condition $\left|{}^{(1)}\mathbf{r}_E - {}^{(0)}\mathbf{r}_E\right| < \varepsilon$ is not fulfilled then we put ${}^{(1)}\mathbf{r}_E = {}^{(0)}\mathbf{r}_E$ and the calculation is repeated from the fourth point,
- $\varphi_3 = \varphi_3 + \Delta\varphi_3$ is chosen and the calculation is repeated from the fourth point.

The compressor housing is simultaneously deformed by a pressure field which acts on the inner walls of the housing. To determine the displacement of the centres of the bearing due to force effects the method of finite elements [2] was used. Boundary conditions of solution are:

- reaction forces in the bearings, Fig. 5,
- pressure in chambers acting on the inner wall of the casing,
- zero displacements of the nodes in places of fixing the compressor housing,
- bearings are considered as rigid as their deformations are determined, see Chapter 1, separated.

The numerical solution to the casing deformation was made using the software ANSYS.

Temperature field

The temperature field was obtained by measurement and estimation. Measurements were carried out at the Technical University in Vienna. The distribution of the temperature field acting on the compressor housing is presented in [2]. Temperature distribution in the longitudinal and in the transverse direction is seen along the lines. Heat housing deformation was made using the software ANSYS and MSC.Marc.

Displacement of the bearing centres

The displacements of bearing centres are presented in **Tab. 1** for three sizes of the angle of rotation φ_3 of the main rotor and shown in **Fig. 6**.

	d_{A_3} [μm]			d_{A_2} [μm]			d_{B_3} [μm]			d_{B_2} [μm]		
	x	y	z	x	y	z	x	y	z	x	y	z
$\varphi_3=0°$ $\equiv 72°$	28,335	-11,187	-56,043	31,796	17,966	-52,534	33,945	-16,196	53,671	36,452	23,082	54,831
$\varphi_3=6°$	28,269	-11,107	-55,956	31,668	17,871	-52,412	33,615	-15,716	53,791	36,183	22,761	54,911
$\varphi_3=12°$	28,128	-11,205	-56,040	31,541	17,659	-52,497	33,254	-15,199	53,745	36,012	22,331	54,851
$\varphi_3=18°$	28,095	-11,031	-56,272	31,488	17,717	-52,775	33,161	-14,370	53,465	35,885	22,241	54,463

Tab. 1 Total displacement of the bearing centres

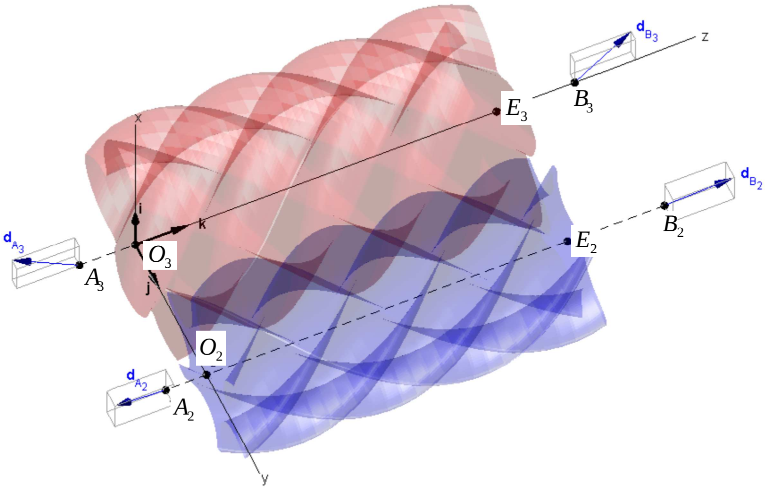

Fig. 6 Displacement of bearing centres

Rotor distortion

The deformation of rotors was done only for the temperature loading. Like the measurement of the screw compressor housing the temperature measurement of rotors was performed at the Technical University of Vienna. Thermal deformations of rotors were designed using software MSC Marc. In the presented solution we assume a perfectly rigid rotors and their deformation due to power and temperature fields are not considered.

3. Contact rotors in working conditions

3.1 Trajectory of bearing centres and position of rotor axes

Position of the bearing mass centres was determined in the twelve time levels which are given by the angle φ_3 of rotation of the main rotor. For continuous analysis of the contact of the surface of rotors at the time interval, the position of the centre bearings was interpolated in cubic spline curve. If we denote the position vectors of the basic points ${}_iX_j^{\Delta}$ of spline curve as

$$\mathbf{r}_{{}_iX_j^{\Delta}} = \mathbf{r}_{{}_iX_j} + \mathbf{d}_{{}_iX_j} \;, \tag{3}$$

where $i = 0, \dots 11;\ j = 2,3;\ x = A, B$ are limiting points of the curve, then the tangent vectors $\mathbf{r}'_{{}_iX_j^{\Delta}}$ in points of the curve $p = p(t),\, t \in \langle t_0, t_{11} \rangle$ are given [5] by the following formula

$$\frac{1}{{}^{i}k}\mathbf{r}'_{{}_{i}X_j^{\Delta}} + \left(\frac{2}{{}^{i}k}+\frac{2}{{}^{i+1}k}\right)\mathbf{r}'_{{}_{i+1}X_j^{\Delta}} + \frac{1}{{}^{i+1}k}\mathbf{r}'_{{}_{i+2}X_j^{\Delta}} = \frac{3}{{}^{i+1}k^2}\,\mathbf{r}_{{}_{i+2}X_j^{\Delta}} + \left(\frac{3}{{}^{i+1}k^2}-\frac{3}{{}^{i+1}k^2}\right)\mathbf{r}_{{}_{i+1}X_j^{\Delta}} - \frac{3}{{}^{i+1}k^2}\mathbf{r}_{{}_{i}X_j^{\Delta}} \quad .(4)$$

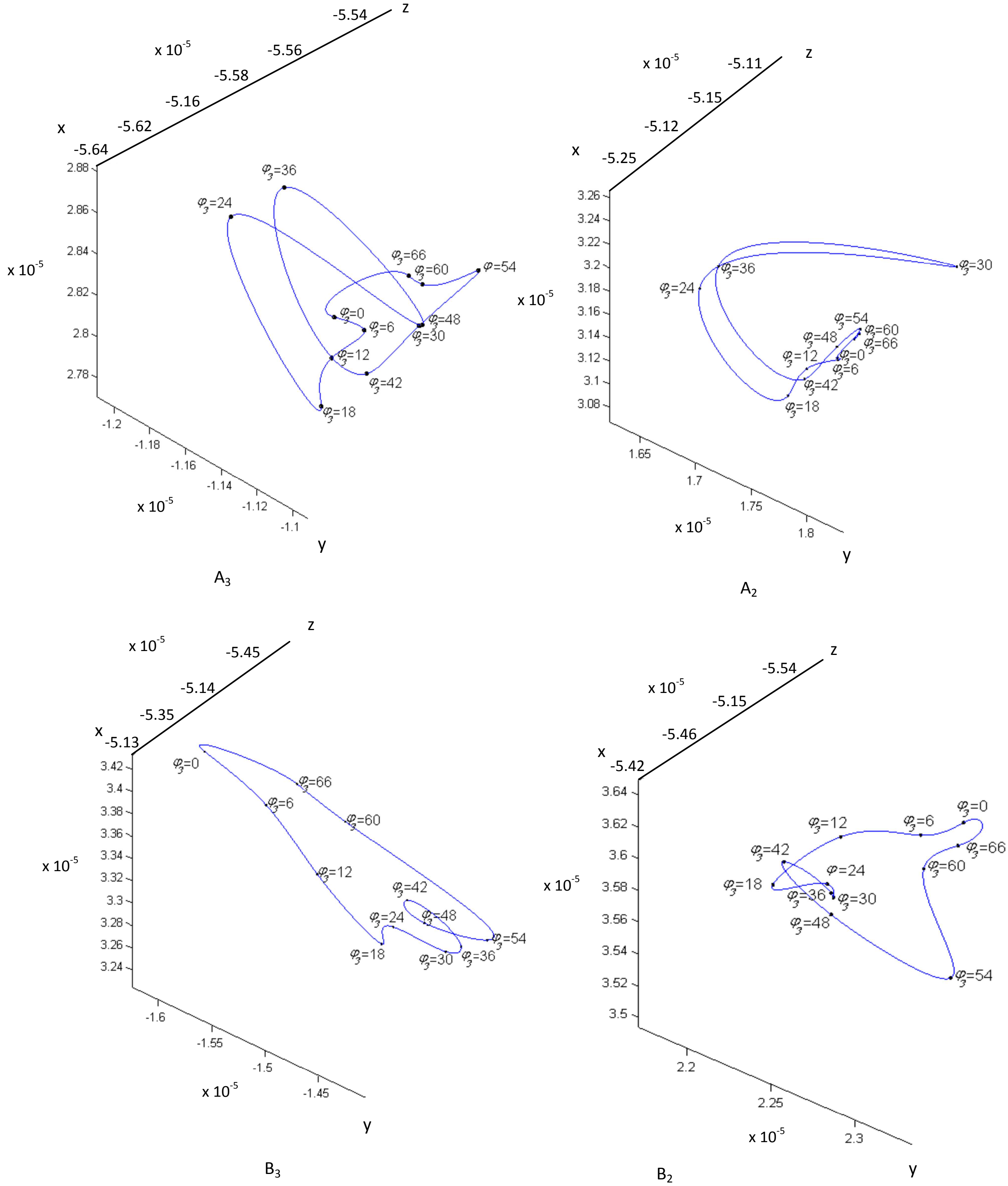

Fig. 7 Trajectories of bearing centres

Individual arcs are given Ferguson´s arches

$$\mathbf{P}(t) = H_0(t-t_i)\mathbf{r}_{_i X_j^{\Delta}} + H_1(t-t_i)\mathbf{r}_{_{i+1} X_j^{\Delta}} + H_2(t-t_i)\mathbf{r}'_{_i X_j^{\Delta}} + H_3(t-t_i)\mathbf{r}'_{_{i+1} X_j^{\Delta}} \quad , \tag{5}$$

where $H_0(s)\ldots\ldots H_3(s)$, $s = t - t_i$, are third – degree polynomials.

Interpolation bearing centres using spline curves are shown in **Fig. 7**. Relative positions of the axes of rotation of the rotors in twelve time levels are shown in **Fig. 8**.

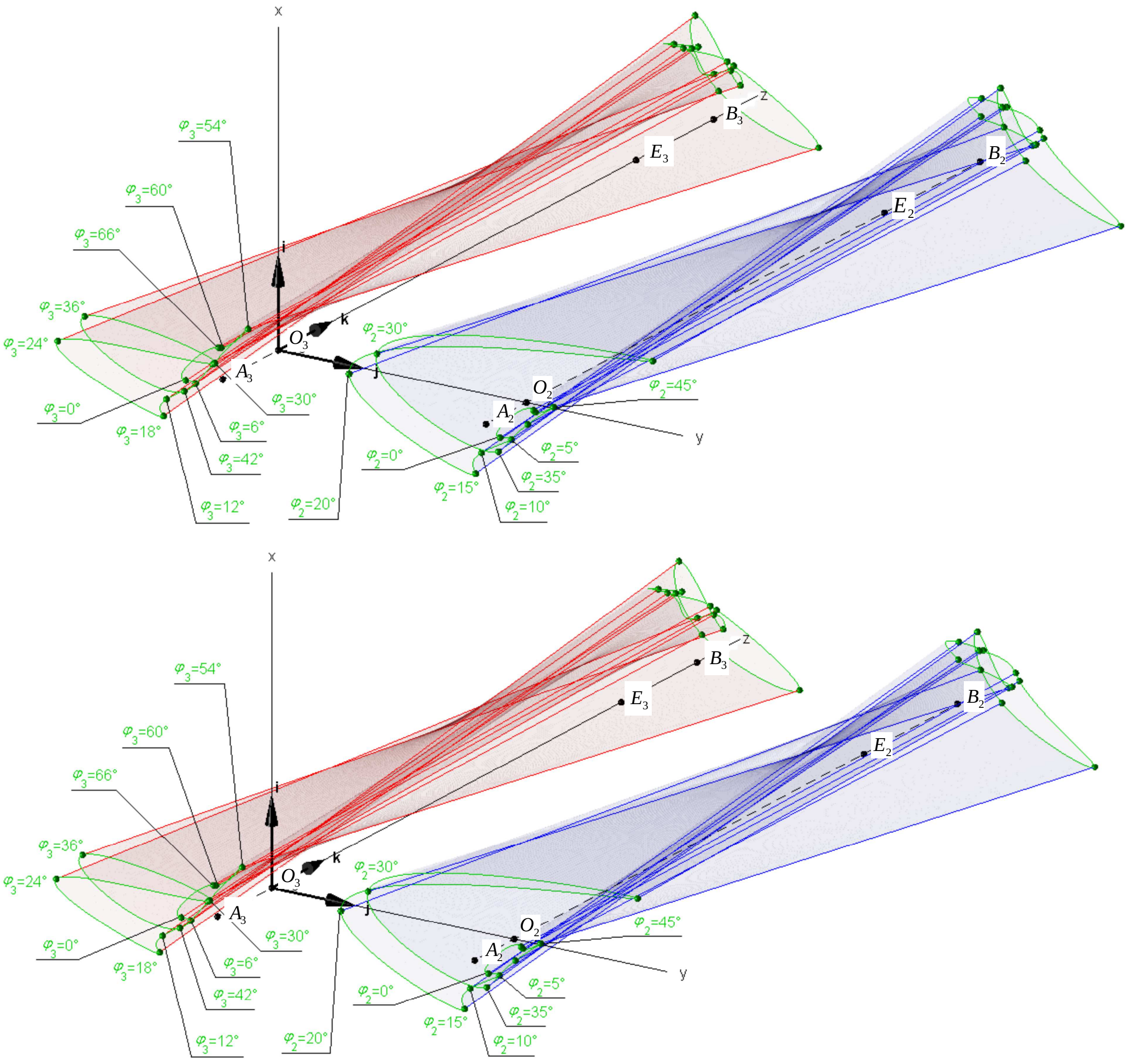

Fig. 8 Relative positions of rotor axes

3.2 Determine the point of contact

Touch point of tooth surface rotors of contact is determined in a way that was shown in [2]. Axis of the gate rotor is in the theoretical position and axis deviations of both rotors are superimposed on the axis of the main rotor. The immediate point of contact of tooth surfaces in the selected position of rotors (φ_3) is determined using set of cutting planes perpendicular to the axis of the female rotor. In every front plane we get the point of contact of tooth profiles. The point of contact of tooth surfaces will be such a point of contact profiles, which needs to realize at a contact the smallest angle of rotation, **Fig. 9**, of the female rotor ${}_n\varphi_2'$, where *n* denotes a pair of meshing surfaces, ${}_{R_2^\Delta}z$ is the displacement along the axis of the female rotor and l is the length of rotors. From figure 9 it is clear that for a given position of rotors (φ_3) the smallest angle of the rotation of the female rotor is on the fourth pair of meshing surfaces. Designation of mating surfaces is shown in **Fig. 10,** where ${}_m\sigma_3$ or

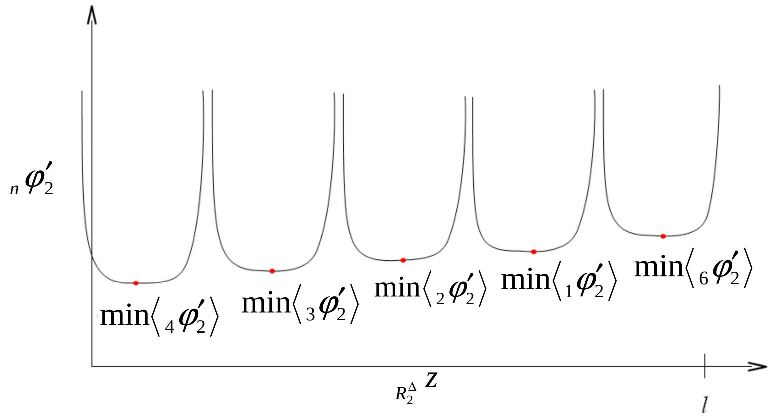

Fig. 9 Dependence ${}_n\varphi_2'$ on the displacement along the axis of the female rotor

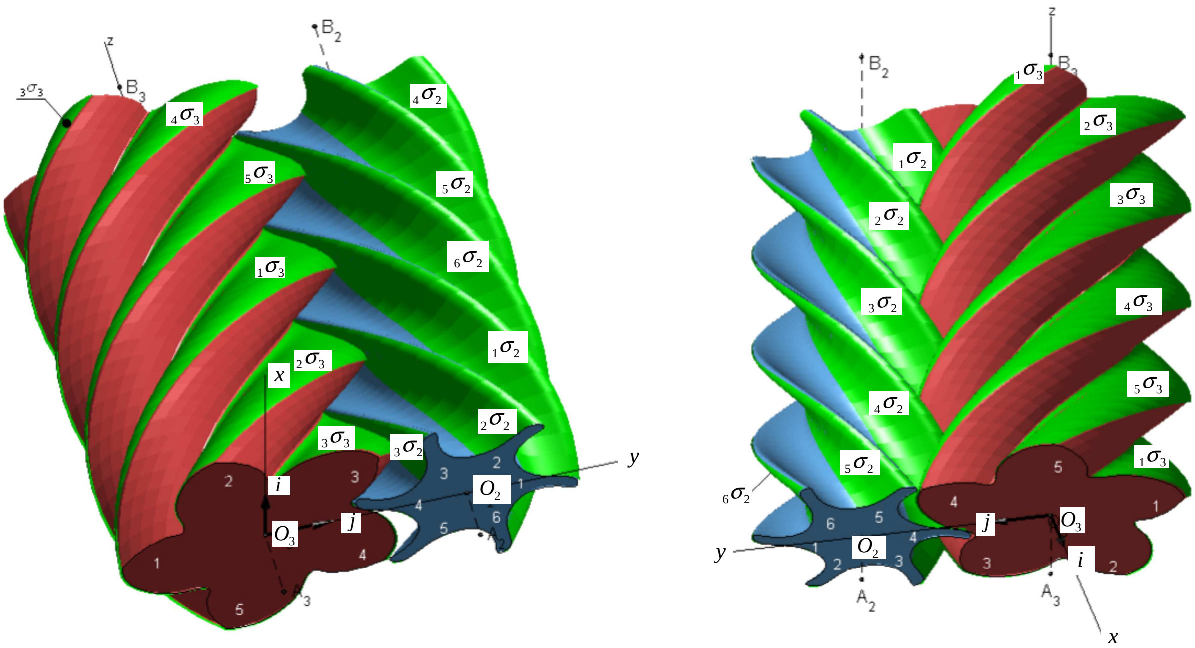

Fig. 10 Designation of conjugate tooth surfaces for the position of the rotor $\varphi_3 = 0^\circ$

${}_n\sigma_2$, $m = 1, 2, ..., 5$, $n = 1, 2, ..., 6$ are the traction surfaces for transmitting rotary motion. The positions of the contact points on all five associated tooth surfaces are shown in **Fig. 11**. It shows the following sequence of time for touch point

$$ {}^{(t_1)}_{k}C = {}^{t_2}_{k+1}C \tag{6}$$

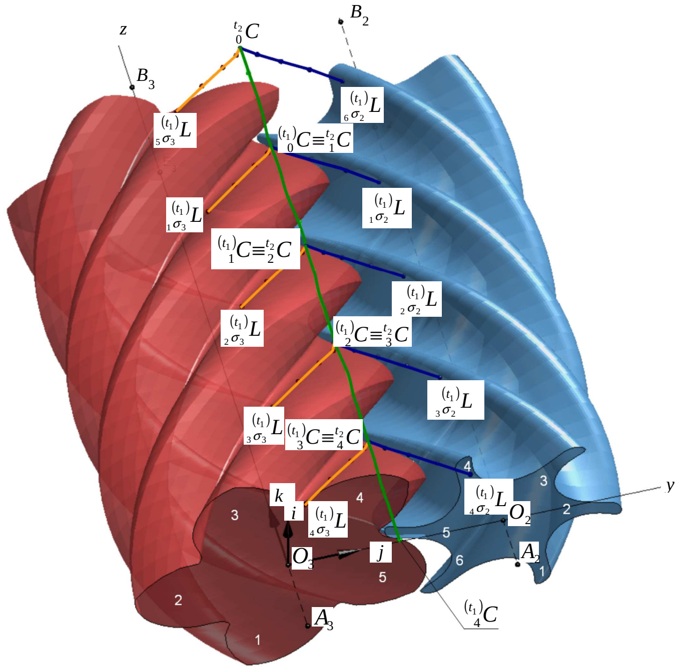

Fig. 11 Location of the touch point on each mating surface

where the left superscript in parentheses denotes the past time and the present time is without brackets. The equation (6) indicates that the point of contact of tooth surfaces in the beginning of the working cycle on the *k*-th pair of teeth is identical to the touch point on the tooth surfaces *k*+1 pair of teeth at the and of the cycle. From Figure 11 it is further seen that in the case of zero pair of teeth $({}_5\sigma_3,\ {}_6\sigma_2)$ and the fourth pair of teeth a part of the trajectory of contact point is outside the real surfaces.

3.3 Movement of the point of contact at the time interval

According to the diagram in **Fig. 12** it could be assumed that all the single cycle will be the contact point on the fourth pair of meshing surfaces. From **Fig. 13**, it is clear that the fourth pair of teeth is negative at the beginning of the z-coordinate. This means that the contact point is located outside the real surface, see Figure 11.

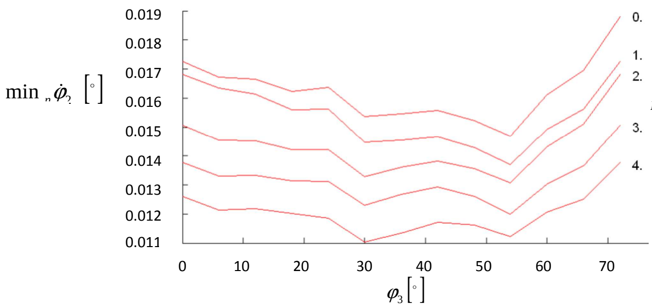

Fig. 12 Dependence $\min {}_{n}\varphi_2'$ on φ_3

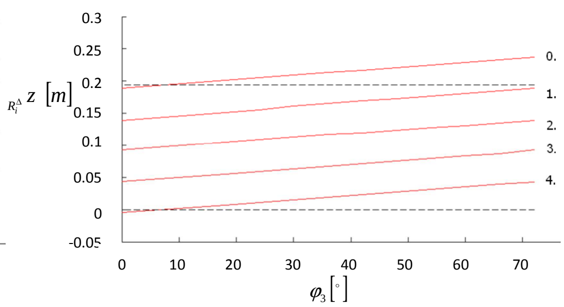

Fig. 13 Dependence $\min {}_{R_2^\Delta} z$ on φ_3

In the first phase the touch point must therefore lie on the third pair of the meshing surfaces up to an angle of rotation φ_3 of the main rotor for which the z – coordinate of the touch point of the fourth pair is zero. Then the point of contact moves from the third pair of teeth on the fourth pair. This situation is illustrated in **Fig. 14**. In the first part of Fig. 14, the contact point ${}^{t_1}C$ of surfaces of the third pair of teeth at time $t_1 = 0$, where the angle of rotation of the main rotor ${}^{1}\varphi_3 = 0^{\circ}$, is shown. The next part of Fig. 14 shows the situation at time t_2 where the

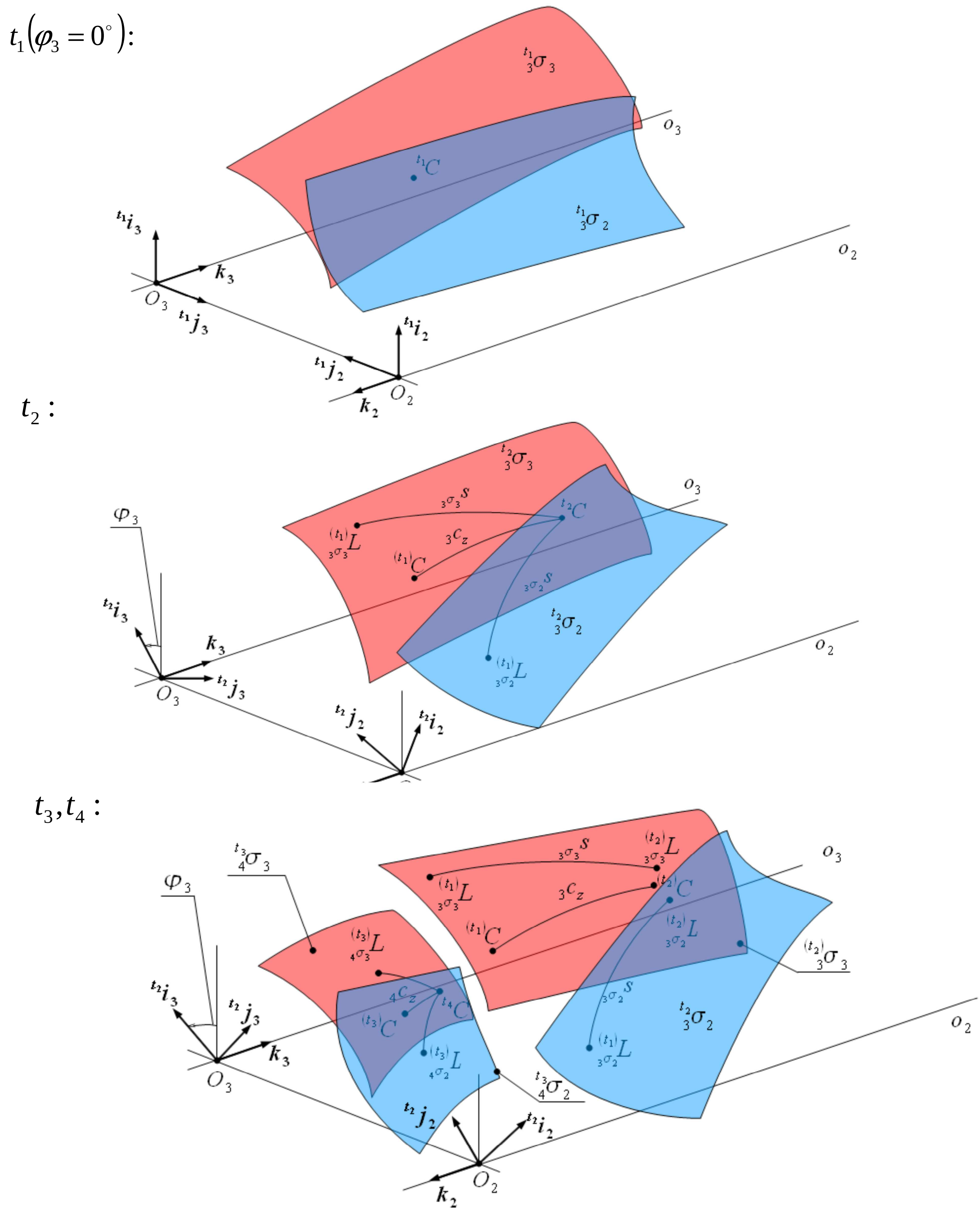

Fig. 14 Trajectory of the point of contact

rotation angle of the main rotor $\varphi_3 = 7{,}4905^\circ$. The touch point ${}^{t_2}C$ moves along the curve ${}_3c_z$ to the limit position. This part of the figure shows also the trajectory ${}_{3\sigma_3}s$ and ${}_{3\sigma_2}s$ on the tooth surfaces of rotors. Upon further rotation of the main rotor to the position ${}^3\varphi_3 = {}^2\varphi_3 + \Delta\varphi_3$, so to the time t_3, the point of contact moves on the next pair of teeth i.e. on the surface ${}_4\sigma_2$ and ${}_4\sigma_3$. This situation is shown in the third part of Fig. 14. During the further rotating of rotors (time t_4) the contact point moves along the meshing curve ${}_4c_z$. Rotation of the main rotor at the angle of 72°, the point of contact goes to the original starting position $\left({}^{t_1}C\right)$ but this time on surfaces of the 4-th pair of teeth and the cycle repeats.

Important is the time t_2 $\left({}^2\varphi_3 = 7.4908^\circ\right)$ when the movement of the point of contact of the third pair of teeth on the fourth pair of tooth surfaces takes place. For a deeper analysis of contact at this time we use spline curves in Figure 7. Using the procedure shown in Fig. 9, we obtain for the third and fourth pair of tooth surfaces and for a rotation angle $\varphi_3 = 1{,}4^\circ$, the situation that is shown in **Fig. 15** where $n = 3,\ 4$. The diagrams in the figure show that at this moment

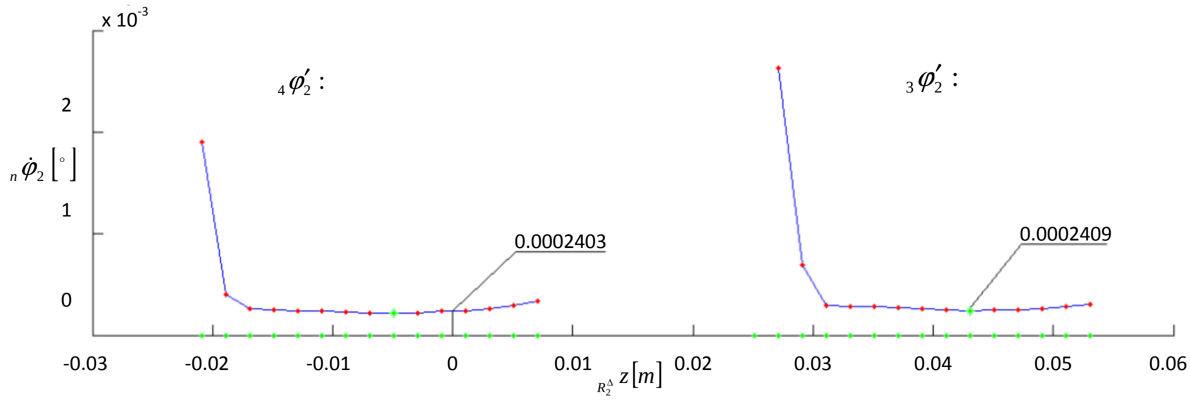

Fig. 15 Dependence $\min\ {}_n\varphi_2'$ on ${}_{R_2^\Delta}z$ for the third and fourth pair of teeth for position $\varphi_2' = 1{,}4^\circ$

the point of contact is simultaneously on the third and fourth pair of tooth surface. Upon further rotation of the main rotor the tooth surface of the third pair is moving away and the point of

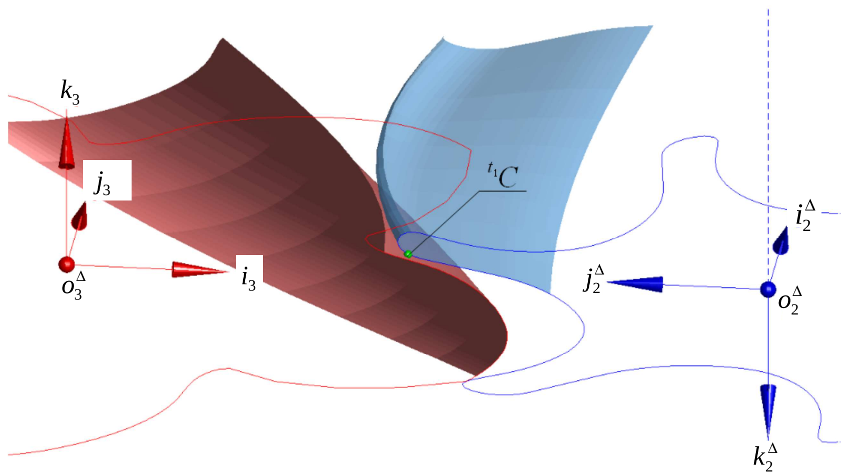

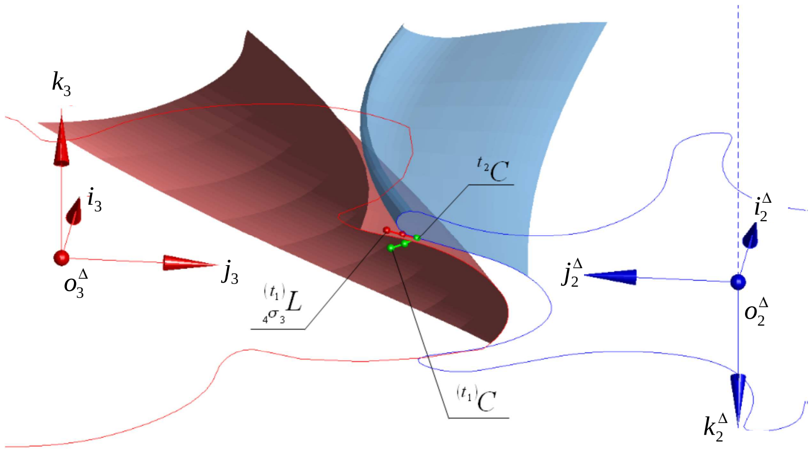

Fig. 16 Movement the point of contact on the edge and surface of the gate rotor

contact remains only on the surfaces of the fourth pair. As a result of the deformation of the rotor housing the main rotor is moved forward the gate rotor and a contact edge of the gate rotor with the main rotor surface takes place. Subsequently the contact oversteps on the surface of the gate rotor. The situation is shown in **Fig. 16**.

4 Conclusion

The paper provides the analysis of the contact of tooth surfaces of the liquid injected screw machines that are in a working state. The aim of the analysis is to show a complicated process by the meshing of rotors that are loaded by force and temperature effects. Change in the contact of rotors leads to a change of the force load of the rotors. That will produce a contact of tooth surfaces of rotors at one point or at two points simultaneously. This situation could be and probably also is, the source of internal excitation of a screw machine. The assumption of perfect stiffness of the rotors is a significant simplification. Consideration of thermal deformation of the rotors can lead to more accurate results or to correcting the presented conclusions.

Acknowledgements

Without the kind support of the Technical University of Dortmund and Department of Mechanics, University of West Bohemia in Pilsen, this article could not have been written.

References

[1] Švígler, J.: A Treatise on the Theory of Higher Kinematic Pair. 13th World Congress in Mechanism and Machine Science. Guanajuato, México, June 2011, IMD-123.

[2] Švígler, J., Machulda, V.: Contact of screw machine rotors under operate loading. VDI Berichte 2101, Schraubenmaschine 2010. VDI Verlag GmbH. Düsseldorf 2010, pp. 345-354.

[3] Švígler, J.: Contribution to the three – dimensional analysis of screw machine rotors. International Conference on Compressors and their Systems, London 2009. Chandos Publishing is an imprint of Woodhead Publishing Limited. Cambridge, UK 2009, pp. 87-97.

[4] Siegl, J.: Modeling of contact bodies. Dissertation thesis, Pilsen 2010.

[5] Kašpar, J.: Analysis of the motion of the rotors screw compressor. Diploma thesis. Pilsen 2012 (In Czech).

[6] Fröhlich, J.: Technika uložení s valivými ložisky, SNTL. Prague 1980 (In Czech).